

STRUCTURIZATION OF COATINGS IN THE PLASMA ARC SPRAYING PROCESS USING $B_4C + (Cr, Fe)_7C_3$ -CORED WIRES

G.M. Grigorenko,¹ L.I. Adeeva,¹ A.Yu. Tunik,^{1,2} V.N. Korzhik,¹
L.K. Doroshenko,¹ Ye.P. Titkov,¹ and A.A. Chaika¹

UDC 621.793.7

The structure and phase composition acquired by coatings deposited in optimum mode by the plasma arc spraying process were examined. The spraying materials were wires with a steel sheath and $nB_4C + 100 - n(Cr, Fe)_7C_3$ cores. The coatings have a ferrite matrix doped with Cr, B, and C and hardened with $Fe_3(B, C)$, Cr_2B , $FeCr$, and boron carbide particles. When the $(Cr, Fe)_7C_3$ amount in the wire increases from 30 to 50 wt.%, the matrix phase (α -Fe-based solid solution) content decreases from 65.8 to 37.6 wt.% and the weight content of the hardening phases increases from 28.2 to 59.3%. These processes improve hardness of the coatings to 6.25 and 8.6 GPa, respectively. All coatings are characterized by a fine lamellar structure and high adhesion to the substrate. They exhibit high density and low porosity (<2.5%) and their hardness exceeds that of the wire steel sheath by 4.0 to 5.5 times. The plasma arc coatings can be used as wear-resistant materials for protection of chemical engineering equipment against abrasive wear, in the production of parts for pumps, compressors, and other machines, and for the recovery of worn parts.

Keywords: plasma arc spraying, cored wire, carbide reinforcement, phase transformations, structure, precipitation hardening of coatings, borides, borocementite, microhardness.

INTRODUCTION

This research effort has been inspired by the advances in plasma spraying processes for depositing coatings of refractory materials and associated composites. The high temperature (to 15000–20000 K) and high speed (to 1000–3000 m/sec and greater) of plasma jets allow them to be considered effective sources of heating, melting, and sputtering for refractory materials. Powders are predominantly used nowadays for gas spraying. Cored wires and rods occupy the second place among the materials for plasma arc spraying (PAS) [1–4]. The cored wires and rods containing refractory compounds are characterized by extensive application. According to the Linde AG Company [5], their annual consumption exceeds 50 kilotons. The use of cored wires for deposition of coatings offers a number of advantages over powders: the process is more energy-effective (specific energy inputs become one-eighth to one-fifteenth in the case of wire coating deposition); the coatings are formed by molten particles (since the wire melts at the instant it enters the high-temperature plasma area and the molten droplets are accelerated to transfer the required kinetic energy to the particles); the process is more stable, etc.

¹E.O. Paton Electric Welding Institute, National Academy of Sciences of Ukraine, Kyiv, Ukraine.

²To whom correspondence should be addressed; e-mail: allatunik@gmail.com.

Translated from Poroshkova Metallurgiya, Vol. 58, Nos. 5–6 (527), pp. 82–97, 2019. Original article submitted February 4, 2019.

The process is further improved by, first, using an anode wire that melts not only with the heat released by the plasma jet but also with the heat released on the anode when electric current passes and, second, by controlling the dynamic gas characteristics of the plasma jet [6–8].

A significant contribution to the development and study of the PAS processes using starting wire materials was made by Ukrainian and CIS scientists such as Kharlamov, Borisov, Petrov, and Pokhmurski [1, 4, 8–10]. The plasma spraying mechanism involving wire materials was examined in detail in [11–14]. The efforts of Japanese researchers, Hasui and Morigaki [15], are noteworthy among foreign papers. There is no significant experience in PAS with cored wires since they were previously used mainly for electric arc spraying [4, 10, 16, 17].

In this effort, we deposited coatings by the high-speed PAS process with a conducting cored wire employing the PLAZER 30PL-W unit developed at the E.O. Paton Electric Welding Institute. The PLAZER PAS process involves an argon arc and intensive air blowing. The arc burns between a tungsten cathode blown round with argon at a low flow rate and a melting conducting wire fed from behind the double-jet plasma arc exit [2, 6, 18].

The E.O. Paton Electric Welding Institute deals with systematic development of cored wires produced from powders of carbides, borides, and other refractory compounds for PAS of coatings to possess high wear resistance and other special properties [19]. We described the features peculiar to the spraying process using wires with a steel sheath and various refractory cores in the papers [20–23].

The objective of this effort is to study the structure, phase composition, and properties acquired by coatings deposited by the plasma arc spraying process using wires with a steel sheath and $B_4C + (Cr, Fe)_7C_3$ powder cores in different proportions.

To improve the wear resistance of various parts operating with limited lubrication and at elevated temperatures and loads, wear-resistant coatings made of cermets—materials produced from metals (alloys) hardened with refractory particles of carbides, borides, carborides, nitrides, silicides, etc.—should be applied.

In our experiment, we introduced refractory B_4C and $(Cr_{0.7}Fe_{0.3})_7C_3$ compounds into the wire core to produce coatings with a precipitation-hardened ferrite matrix. Boron carbide is widely used in modern technology both in pure form and as cermets since it possesses unique properties (49.5 GPa hardness, high wear resistance, and high chemical stability). The interaction of boron carbide with a ferrite wire sheath is determined by the chemical affinity of iron for boron and carbon. The interaction in the Fe–B–C system heated in a protective gas atmosphere first leads to iron borides, FeB and Fe_2B , and then to cementite, Fe_3C [24]. At high temperatures, boron carbide contacts with steel to dope it with boron and carbon. In the process, boron carbide partially or fully decomposes, doping the ferrite matrix and forming fine iron boride and carboride phases [25]. At B_4C content up to 10 wt.%, the matrix acquires a fine-grained structure including carbide particles that do not form the skeleton. These materials show high strength ($\sigma_b = 700$ MPa) [24–26].

Compound Cr_7C_3 is one of the three stable carbides (Cr_3C_2 , Cr_7C_3 , $Cr_{23}C_6$) that are known to exist in the Cr–C system and contain 13.34, 9.00, and 5.68 wt.% C. The hardness of Cr_3C_2 and Cr_7C_3 is comparable: 18 and 18.8 GPa [27]. Chromium carbide Cr_3C_2 shows higher oxidation resistance than lower carbides Cr_7C_3 and $Cr_{23}C_6$. But coatings made of the lower chromium carbides have higher chemical stability and equal or even greater wear resistance than the Cr_3C_2 coatings. In the spraying process, interaction occurs between the steel sheath and powder cores to form new phases of complex composition since iron and chromium have unlimited solubility and can substitute each other in chemical compounds. Complex carbide $(Cr_{0.7}Fe_{0.3})_7C_3$ introduced into the core additionally dopes the matrix with chromium and thus increases its high-temperature oxidation resistance. Moreover, this carbide can react with B_4C to form new hardening phases such as complex carborides.

EXPERIMENTAL PROCEDURE

The coatings were deposited using the PLAZER-30 unit [17, 19] in two modes: at a plasma arc current of 210 A (mode 1) and 240 A (mode 2). Other spraying parameters were the same: voltage $U = 60$ V, air flow rate $Q_{air} = 45$ L/min, argon flow rate $Q_{Ar} = 30$ L/min, and spraying distance $d = 175$ mm.

The starting materials and plasma-deposited coatings were examined employing a comprehensive procedure including: metallography, hardness measurement (loads of 0.25, 0.5, and 3.0 N), and X-ray diffraction (XRD) with a DRON-UM1 diffractometer. The structure and elemental composition of the coatings were determined by electron microprobe analysis (EMPA) employing an analytical system consisting of a JSM-35 CF scanning electron microscope (SEM) (JEOL, Japan) and an INCA Energy-350 energy-dispersive spectrometer (Oxford Instruments, Great Britain). This procedure is peculiar in that the analysis is highly local (excitation region is 1 μm). The structure was photographed in secondary electron image (SEI) mode at $U = 20$ kV. Differential thermal analysis (DTA) was carried out using a VDTA-8M unit in a helium atmosphere. The cored wires were examined in the same heating and cooling conditions ($T_{\text{max}} = 1600^\circ\text{C}$, $V = 80^\circ\text{C}/\text{min}$) to determine their melting and crystallization points and temperature ranges of solid-state phase transformations. The samples were heated and cooled twice. The primary thermal curve corresponds to heating (cooling) of the starting sample and the secondary thermal curve describes heating of the sample after being melted in the crucible (to produce an ingot or sinter). This paper shows DTA curves for the second heating and cooling event as they more accurately reflect the physical processes that occur in the test materials.

To reveal the structure of the test materials, we used chemical etchants. The Nital etchant (4% alcoholic nitric acid solution, $\tau = 5\text{--}30$ sec, $t = 20^\circ\text{C}$) exposed the iron-based matrix and a 10% alcoholic iodine solution ($\tau = 5\text{--}15$ sec, $t = 20^\circ\text{C}$) exposed the boride component.

EXPERIMENTAL MATERIALS

For plasma arc spraying of protective cermet coatings, we used wires with different cores, wt.%: 70 B_4C + 30 $(\text{Cr}_{0.7}\text{Fe}_{0.3})_7\text{C}_3$ and 50 B_4C + 50 $(\text{Cr}_{0.7}\text{Fe}_{0.3})_7\text{C}_3$. The powder core amount in the wire was varied between 12.5 and 15.6 wt.% of the wire total weight. The wire diameter was 1.8 mm. The characteristics of wire core materials are summarized in Table 1. The wire sheath was made of low-carbon steel (St08kp), wt.%: 99.2 Fe, 0.45 Cr, 0.2 Al, 0.2 Mn, and 0.08 C. The microhardness of St08kp steel was 1.55 ± 0.70 GPa. The coatings were deposited onto a low-carbon steel substrate with a microhardness of 1.90 ± 0.2 GPa.

TABLE 1. Characteristics of Wire Core Materials

Material	Particle (grain) size, μm	Microhardness, $HV0.25$, GPa	Phase composition according to XRD, wt.%
Boron carbide	40–100	29.96 ± 3.06	92.3 B_4C + 7.7 C
Double chromium–iron carbide	10–100	18.80 ± 1.56	$\sim 100 (\text{Cr}_{0.7}\text{Fe}_{0.3})_7\text{C}_3$
St08kp	4–20	1.55 ± 0.7	$\sim 100 \alpha\text{-Fe}$

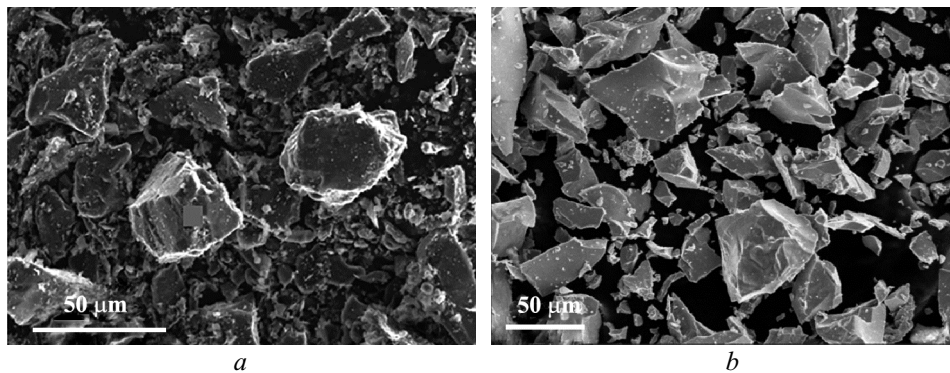


Fig. 1. Morphology of the B_4C (a) and $(\text{Cr}_{0.7}\text{Fe}_{0.3})_7\text{C}_3$ (b) powder cores

The B₄C powder produced by grinding an ingot consists of irregular splintery particles 40–100 μm in size (Fig. 1a). The powder particles had a microhardness of 21.40–35.00 GPa. According to XRD, B₄C is the main powder phase with lattice parameters $a = 0.56078$ nm and $c = 1.20897$ nm; there is also a small amount of carbon with hexagonal lattice parameters $a = 0.24658$ nm and $c = 0.67849$ nm.

The (Cr_{0.7}Fe_{0.3})₇C₃ powder represents a complex carbide produced by ingot grinding (Fig. 1b). The powder particles are dense and of irregular splintery shape; their size is 50–200 μm and microhardness is 16.93–24.90 GPa. This powder contains 62.5 wt.% Cr, 28.7 wt.% Fe, and 8.8 wt.% C.

SIMULATION OF THERMODYNAMIC INTERACTION BETWEEN WIRE COMPONENTS IN THE HEATING PROCESS

Using DTA data, we simulated the thermodynamic interaction between the wire components in the spraying process. The composition of the cored wires under study is shown in Table 2. Analysis of phase transformations in the simulated ingots allows us to predict, to a certain extent, the formation of phases in the coatings if the material being sprayed is adequately protected against decarbonization, oxidation, and other processes that accompany spraying.

Figure 2 shows thermal curves plotted in the second heating (1) and cooling (2) event since they more accurately represent the physical processes that occur in the materials being sprayed.

We examined wires with different ratios of the two core components. The DTA ingot made of a 70 B₄C + 30 (Cr, Fe)₇C₃-cored wire melts in several stages as shown on the thermal curve (curve 1 in Fig. 2a). An endothermic bend, along which the eutectic melts, is observed in the range 1150–1270°C. Then the high-temperature component melts in two stages in the range 1300–1400°C. The liquidus and solidus temperatures of the sample are $T_L = 1150$ °C and $T_S = 1320$ °C.

When the sample cools down (curve 2 in Fig. 2a), it crystallizes in two stages: stage 1 is crystallization of the high-temperature ingot part at $T = 1320$ – 1230 °C and stage 2 is crystallization of the low-melting-point component

TABLE 2. Composition of Cored Wires and DTA Results for Simulated Ingots

Core composition, wt.%	Powder core amount, wt.%	T_{melt} , °C	ΔT_L , °C	T_{cryst} , °C	ΔT_S , °C	Ingot phase composition, wt.%
70 B ₄ C + 30 (Cr, Fe) ₇ C ₃	12.5	1150–1320	170	1320–1120	200	87.6 (Cr, Fe) ₇ C ₃ + 12.4 Fe ₂ B
50 B ₄ C + 50 (Cr, Fe) ₇ C ₃	15.6	1140–1350	210	1340–1120	220	96.0 (Cr, Fe) ₇ C ₃ + 4.0 Fe ₂ B

Note: The wire sheath is low-carbon steel.

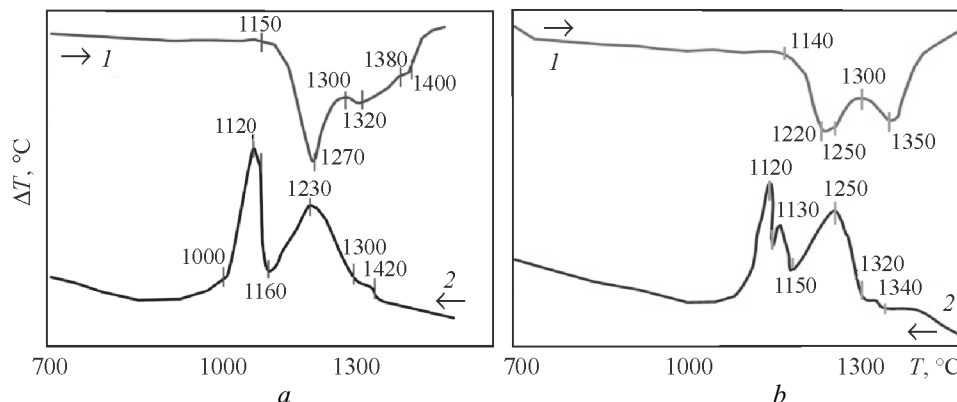


Fig. 2. Thermal heating (1) and cooling (2) curves for DTA ingots produced from wires with 70 B₄C + 30 (Cr, Fe)₇C₃ (a) and 50 B₄C + 50 (Cr, Fe)₇C₃ (b) cores

(eutectic) at $T = 1160\text{--}1120^\circ\text{C}$. The high-temperature ingot part crystallizes in two stages, with a small bend at $T = 1300^\circ\text{C}$. The first stage involves crystallization of the most refractory component and the second stage involves crystallization of the matrix (solid solution) at $T = 1300\text{--}1230^\circ\text{C}$, the matrix area under the exothermic bend being much greater than the refractory area. Crystallization of the eutectic component is observed at $T = 1160\text{--}1120^\circ\text{C}$ (curve 2 in Fig. 2a). The liquidus and solidus temperatures are $\Delta T_L = 170^\circ\text{C}$ and $\Delta T_S = 200^\circ\text{C}$ (Table 2).

As in the previous case, the thermal curve of the $50 \text{ B}_4\text{C} + 50 (\text{Cr, Fe})_7\text{C}_3$ -cored ingot (curve 1 in Fig. 2b) shows endothermic effects associated with ingot melting in the range $1140\text{--}1350^\circ\text{C}$. There are clear bends corresponding to the melting of the low- and high-temperature components. The process begins with the melting of two eutectics in the ranges $1140\text{--}1220^\circ\text{C}$ and $1220\text{--}1250^\circ\text{C}$. Then the high-temperature component melts in the range $1300\text{--}1350^\circ\text{C}$. The solidus and liquidus temperatures are $T_S = 1340^\circ\text{C}$ and $T_L = 1140^\circ\text{C}$ (Fig. 2b, Table 2).

When the $50 \text{ B}_4\text{C} + 50 (\text{Cr, Fe})_7\text{C}_3$ -cored sample cools down (curve 2 in Fig. 2b), the high-temperature component crystallizes in two stages. The thermal curve shows two exothermic bends in the range $1340\text{--}1250^\circ\text{C}$. This process occurs in two stages, a small bend being observed at $T = 1320^\circ\text{C}$. At temperatures ranged from 1150 to 1120°C , the low-temperature component crystallizes in two stages as well: the thermal curve has two bends, at $1150\text{--}1130^\circ\text{C}$ and $1130\text{--}1120^\circ\text{C}$. They are likely to correspond to the crystallization of the double eutectic. Hence, the sample crystallizes in a complex manner over a wide temperature range ($\Delta T_S = 220^\circ\text{C}$).

Both DTA ingots are rather porous; their microstructure includes a light matrix with dark inclusions of geometric shape (Fig. 3). The dark inclusions are elongated and coarse at the ingot center and become finer close to the edges.

After etching, the light matrix shows grains with dark rims, representing a eutectic structure. The rims at grain boundaries are discontinuous and differ in color from the coarse dark inclusions (Fig. 3b, d). Light matrix areas are seen inside the dark inclusions. The matrix has a microhardness of $10.60 \pm 0.42 \text{ MPa}$ and $8.97 \pm 0.72 \text{ MPa}$ and the dark inclusions of $15.05 \pm 1.35 \text{ MPa}$ and $13.67 \pm 2.12 \text{ MPa}$ for the ingots with 30 and 50% $(\text{Cr, Fe})_7\text{C}_3$.

According to XRD and EMPA, the DTA ingots made of cored wires consist of two phases and include boron cementite and iron boride. Both ingots have a $\text{Fe}_3(\text{B}_{0.7}\text{C}_{0.3})$ borocementite matrix doped with 1.5 and 3.0% Cr,

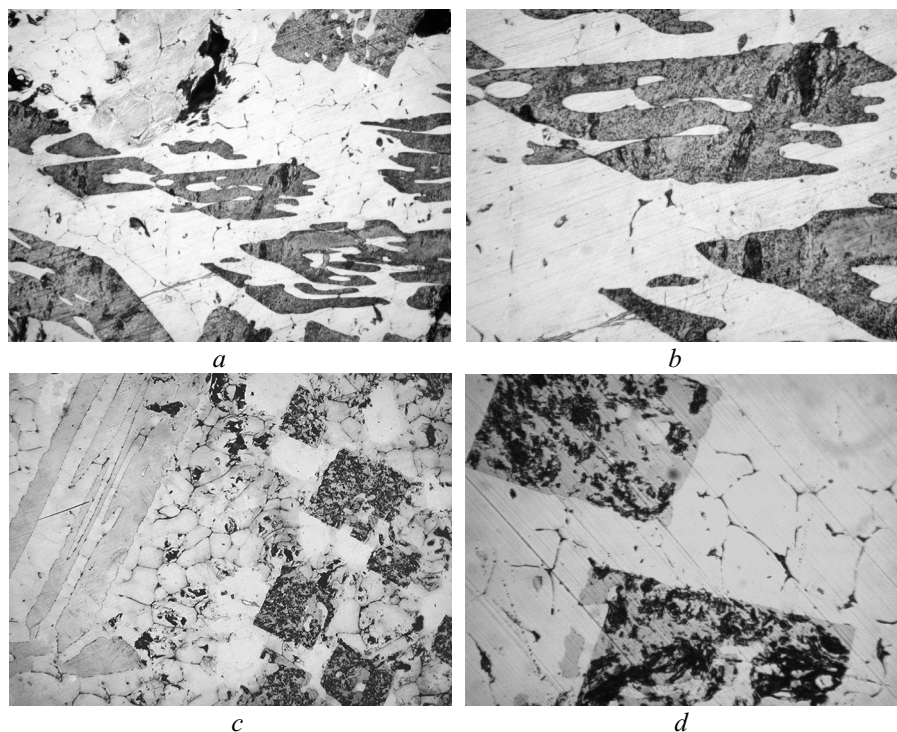


Fig. 3. Microstructure of DTA ingots produced from wires with $70 \text{ B}_4\text{C} + 30 (\text{Cr, Fe})_7\text{C}_3$ (a, b) and $50 \text{ B}_4\text{C} + 50 (\text{Cr, Fe})_7\text{C}_3$ (c, d) cores; $\times 200$ (a, c) and $\times 500$ (b, d) magnification; etched

which is the main phase constituting 87.6 and 96.0%. The dark inclusions are Fe₂B doped with 2.0 and 5.5% Cr. The matrix and dark inclusions contain up to 1% Si. The rims at matrix grain boundaries contain a higher amount of Si (2.0 and 7.0%) and Cr (0.5 and 2.6%) in the ingots with 30 and 50 wt.% chromium carbide.

New phases, such as chromium and iron borides, carbides, and carboborides, may form in interactions in the Fe–Cr–B–C system. Chromium has a higher affinity for carbon and boron than iron does. Therefore, chromium borides and carbides form first and then iron borides and double chromium–iron carbides show up. Inasmuch as the steel wire sheath constitutes more than 80% of the ingot, the sample acquires an iron borocementite matrix containing chromium-doped iron borides.

STUDY OF PAS COATINGS

The coatings show a lamellar, discrete, and inhomogeneous structure. Round particles with oxide rims at boundaries and pores are rare. The lamellas have a high shape factor (length-to-width ratio) since they deform significantly in the deposition process and the coatings thus have lower porosity. The round particles, which obviously cooled down in the spraying process, disturb the lamellar structure and lead to pores. The coatings are distinguished by high quality: they are dense, adhere well to the substrate, and have no cracks or delamination.

When the steel wire with 70 B₄C + 30 (Cr, Fe)₇C₃ and 50 B₄C + 50 (Cr, Fe)₇C₃ cores is subjected to a plasma jet, the molten steel sheath interacts with the refractory core powders to result in defect-free lamellar coatings that have high density and adhere well to the substrate.

Table 3 summarizes the compositions of the cored wires and characteristics of the coatings.

When a plasma jet acts on the material being sprayed—a 70 B₄C + 30 (Cr, Fe)₇C₃-cored steel wire—the wire components interact with each other to form coatings 500 and 600 μm thick in spraying modes 1 and 2 (Fig. 4). The microhardness of the coatings is *HV*3 = 5.41 ± 0.55 GPa and 6.25 ± 0.98 GPa. The coatings primarily consist of lamellas with oxide rims 1–2 μm thick at their boundaries. Round oxide particles that cool down before colliding with the sprayed surface are rarely observed. Their size varies from 15 to 30 μm and amount does not exceed 5.3 vol.%. Dark-gray lamellas are observed in unetched state; they are probably starting boron and chromium carbide particles. Their size is 20–50 μm. The oxide component is presented by individual particles and layers along the lamellar boundaries and is found in a greater amount in the coatings sprayed at a lower plasma arc current (Table 3, Figs. 4 and 5).

TABLE 3. Characteristics of Plasma-Deposited Coatings Produced from Cored Wires with Low-Carbon Steel St08kp Sheaths

Composition of the wire core, wt.%	<i>I</i> , A	Coating thickness, μm	Phase composition according to XRD*	<i>HV</i> 0.5, GPa	<i>HV</i> 3, GPa	Porosity, vol.%	Content of oxide component, vol.%
70 B ₄ C + 30 (Cr, Fe) ₇ C ₃	210	600	69.5 α-Fe; 13.6 FeCr; 5.9 Fe ₃ (B, C); 5.7 B ₄ C; 5.3 B ₆ O	4.56±0.63	5.41±0.55	<2.0	5.3
	240	500	65.8 α-Fe; 12.9 FeCr; 0.9 Fe ₃ (B, C); 5.40 B ₄ C; 5.0 B ₆ O	4.68±0.99	6.25±0.98	<2.5	5.0
50 B ₄ C + 50 (Cr, Fe) ₇ C ₃	210	320	41.9 α-Fe; 18.3 Cr ₂ B; 13.7 FeCr; 11.4 Fe ₃ (B, C); 11.4 B ₄ C; 3.2 B ₆ O	5.14±1.14	6.92±0.56	<1.5	3.2
	240	350	37.6 α-Fe; 20.3 Fe ₃ (B, C); 16.4 Cr ₂ B; 12.3 FeCr; 10.3 B ₄ C; 2.9 B ₆ O	7.86±1.36	8.59±0.89	<1.0	2.9

* The phases are arranged according to decreasing intensities of X-ray peaks.

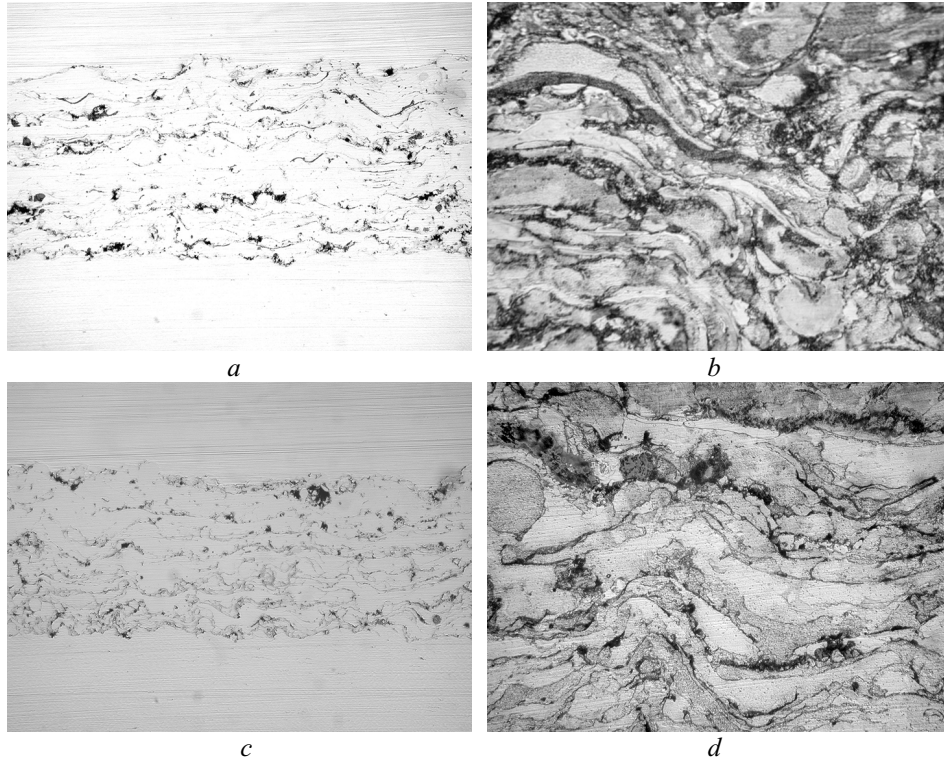


Fig. 4. Microstructure of the plasma-deposited coating produced from a wire with a 70 B₄C + 30 (Cr, Fe)₇C₃ core at a plasma arc current of 210 (*a, b*) and 240 (*c, d*) A; ×100 magnification (*a, c*), unetched, and ×500 magnification (*b, d*), etched

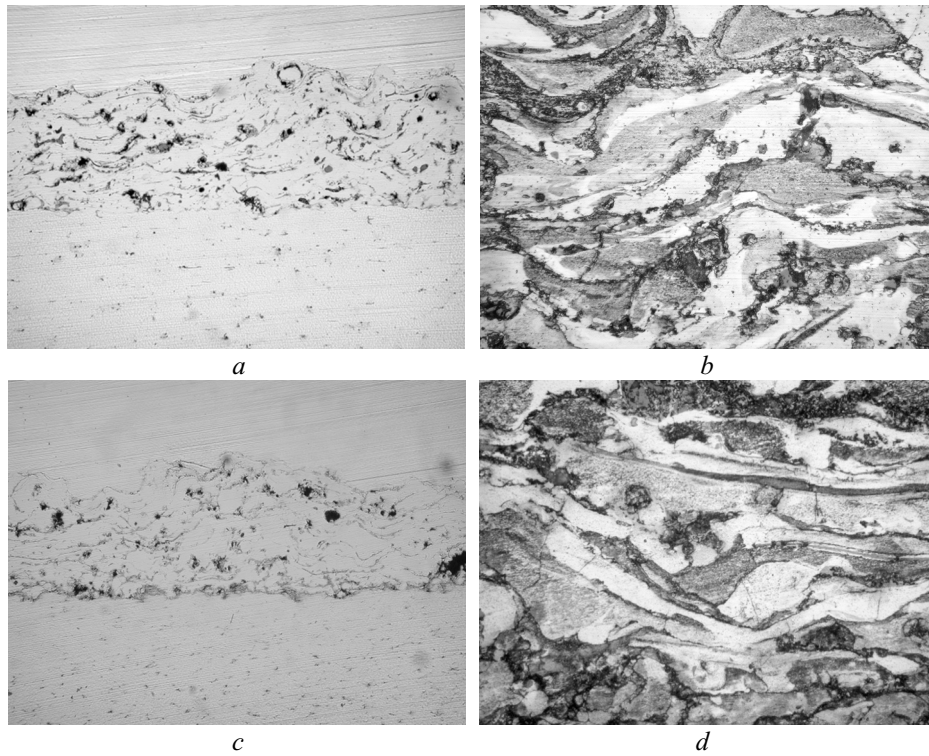


Fig. 5. Microstructure of the plasma-deposited coating produced from a 50 B₄C + 50 (Cr, Fe)₇C₃-cored wire at a plasma arc current of 210 (*a, b*) and 240 (*c, d*) A; ×100 magnification (*a, c*), unetched, and ×500 magnification (*b, d*), etched

After etching, lamellas varying from white to different shades of gray (Fig. 4b, d) were observed because the structural components had different etchability. The white lamellas $45\ \mu\text{m} \times 125\ \mu\text{m}$, $15\ \mu\text{m} \times 35\ \mu\text{m}$, and $20\ \mu\text{m} \times 375\ \mu\text{m}$ in size (shape factors 3–10 and 4–19 for modes 1 and 2) and round particles $7\text{--}35\ \mu\text{m}$ in diameter, whose amount in the coating is $\sim 5\ \text{vol.}\%$, are located between the gray lamellas and round particles in the coating. The gray coating component is predominant, its lamellas being $15\ \mu\text{m} \times 175\ \mu\text{m}$, $20\ \mu\text{m} \times 175\ \mu\text{m}$, and $15\ \mu\text{m} \times 275\ \mu\text{m}$ in size (shape factors 9–12 and 5–18 for modes 1 and 2).

High shape factors of the lamellas are indicative of good heating and high speed of the particles being sprayed. The lamellas, especially light-gray ones, have precipitation-hardening inclusions. The white coating component with the highest doping content has a microhardness of $9.86 \pm 1.25\ \text{GPa}$ and $8.95 \pm 1.75\ \text{GPa}$ and the light-gray lamellas with particulate inclusions have a microhardness of $6.51 \pm 0.60\ \text{GPa}$ and $6.73 \pm 0.80\ \text{GPa}$ for spraying modes 1 and 2. The gray lamellas in the coating have a microhardness of $4.81 \pm 0.55\ \text{GPa}$ and $5.90 \pm 0.85\ \text{GPa}$ and the dark-gray lamellas have a microhardness of $3.96 \pm 0.55\ \text{GPa}$ and $4.94 \pm 0.85\ \text{GPa}$ for spraying modes 1 and 2.

The coatings deposited from a cored steel wire in the same PAS conditions but at a different ratio of core components, $50\ \text{B}_4\text{C} + 50\ (\text{Cr}, \text{Fe})_7\text{C}_3$, have no defects either and do not separate from the substrate (Fig. 5). The coatings are 320 and $350\ \mu\text{m}$ thick and their microhardness HV_3 is $6.92 \pm 0.56\ \text{GPa}$ and $8.59 \pm 0.89\ \text{GPa}$ for modes 1 and 2. In unetched state (Fig. 5a, c), the coatings contain a small amount of the oxide component, $3.2\ \text{vol.}\%$, as thin oxide layers $0.5\text{--}2\ \mu\text{m}$ thick along the boundaries of lamellas and individual oxide particles $1\text{--}10\ \mu\text{m}$ in size. There are also black inclusions and lamellas of the starting boron carbide particles up to $50\ \mu\text{m}$ in size. Their amount is $\sim 7\ \text{vol.}\%$ and microhardness is $18.5\text{--}25\ \text{GPa}$. These inclusions represent partially decomposed boron carbide $\text{B}_{2.8}\text{C}\text{--}\text{B}_3\text{C}$ doped with $18\text{--}41\ \text{wt.}\%$ Cr and $11\text{--}18\ \text{wt.}\%$ Fe; this probably results from interaction of the ferrite matrix and boron carbide. These particles are commonly surrounded by a transition zone whose structure differs from that of the coating matrix and contains an increased amount of boron, carbon, and chromium, thus representing borocementite. There are $\sim 2.9\ \text{wt.}\%$ C, $\sim 11.2\ \text{wt.}\%$ B, and $\sim 4.2\ \text{wt.}\%$ Cr at a distance of $0.4\ \mu\text{m}$ from the carbide (Fig. 6). According to XRD, the coating deposited in the optimum mode contains a number of borocementite areas ($\sim 20\ \text{wt.}\%$). The boron carbide particles observed in the matrix either partially dissociate or interact with $(\text{Cr}, \text{Fe})_7\text{C}_3$ to form complex borides $(\text{Cr}, \text{Fe})_2\text{B}$.

Etching revealed the lamellar structure of the coatings (Fig. 5b, d), including lamellas varying from white to different shades of gray as in the previous sample. The shape factor of the coating particles increases with heat input and is $2.5\text{--}10$ and $3\text{--}15$ for modes 1 and 2. Besides lamellas, the coating matrix has round particles ranging from 10 to $50\ \mu\text{m}$ in size.

The matrix structural components are characterized by different etchability and microhardness, which is associated with their doping content. The microhardness of the white lamellas with the highest doping content is

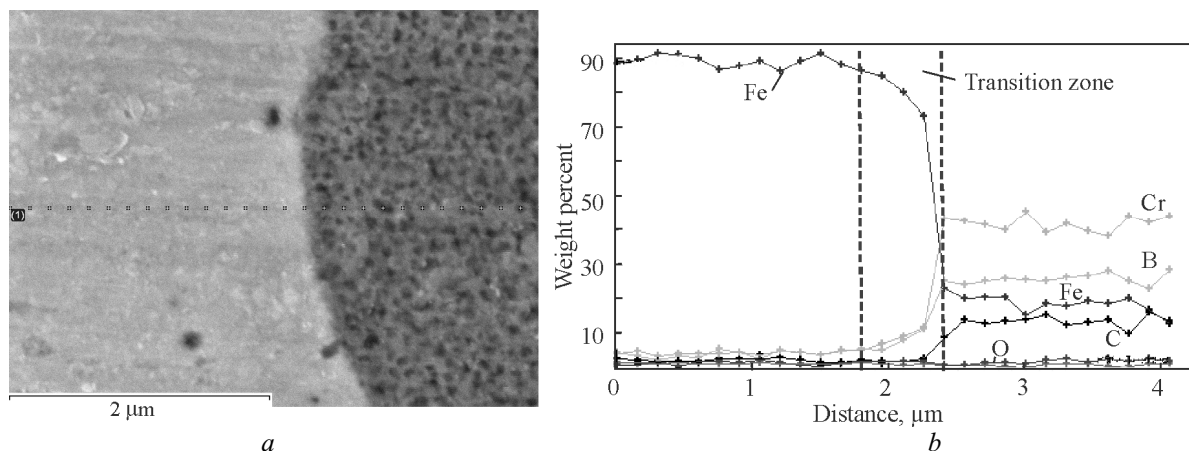


Fig. 6. Contact area between a boron carbide particle and the matrix (a) and distribution of chemical elements (b) in the coating produced from a $50\ \text{B}_4\text{C} + \text{B}(\text{Cr}, \text{Fe})_7\text{C}_3$ -cored wire (mode 2)

6.65 ± 1.15 GPa and 9.54 ± 0.65 GPa. Lower microhardness is shown by the light-gray (4.95 ± 0.15 GPa and 7.14 ± 0.55 GPa) and gray (4.20 ± 0.20 GPa and 6.08 ± 0.40 GPa) lamellas. The softest, dark-gray matrix components have a microhardness of 3.66 ± 0.15 GPa and 3.92 ± 0.95 GPa for spraying modes 1 and 2.

The coating deposited in spraying mode 2 was examined in more detail by EMPA. The smooth white areas contain a significant amount of doping elements, 2.8–3.8 wt.% B, 1.6–4.0 wt.% C, and 1.0–4.3 wt.% Cr, and represent iron borocementite. The light-gray and gray lamellas contain up to 1.8 wt.% B and Cr and 2.0–3.6 wt.% C and the intensively etched dark-gray lamellas contain up to 0.1 wt.% B, 2.1–2.5 wt.% C, and 0.5–1.3 wt.% Cr. Some light-gray and gray lamellas contain particulate inclusions, their highest amount being revealed in spraying mode 2.

The phase composition of the coatings deposited from the 70 B₄C + 30 (Cr, Fe)₇C₃ wire in modes 1 and 2 does not change qualitatively. The X-ray diffraction patterns show the following phases: α-Fe, FeCr, Fe₃(B, C), B₄C, and B₆O (Table 3). However, the amount of borocementite Fe₃(B, C) almost doubled (increased from 5.9 to 11.0%) with a simultaneous decrease in the amounts of doped ferrite and starting (Cr, Fe)₇C₃ and B₄C phases by 3.7, 0.7, and 0.4 wt.% at a higher plasma arc current. The amount of the oxide phase decreased insignificantly (by 0.3 wt.%) from 5.3 to 5.0 wt.%.

Therefore, higher plasma arc current (greater heat input) enhances the interaction between wire components, which increases the amount of the newly formed hardening borocementite phase by 5.0 wt.% and leads to additional doping of the ferrite matrix with B, C, and Cr; this is evidenced by an increase in the α-Fe bcc lattice parameter from 0.28664 to 0.28717 nm.

According to XRD, when the chromium carbide amount increases to 50% in the wire core, Cr₂B phase shows up besides the above-mentioned phases. The presence of chromium boride in the coating with a smaller amount of (Cr, Fe)₇C₃ in the core is attributed only to the predominant content of the iron-based component. The coatings sprayed from the 50 B₄C + 50 (Cr, Fe)₇C₃-cored wire in two modes consist of the following phases: α-Fe, Cr₂B, FeCr, Fe₃(B, C), B₄C, and B₆O (Table 3). With greater thermal input in transition from mode 1 to mode 2, the borocementite amount increases significantly (by 1.8 times), from 11.4 to 20.5 wt.%. The amounts of all other phases decrease. The α-Fe matrix phase content decreases most significantly (by 4.3 wt.%). The α-Fe phase lattice parameter increases from 0.28655 to 0.28717 nm, probably because of higher doping. The amounts of chromium boride Cr₂B, ferrochrome, and boron carbide B₄C decrease by 1.9, 1.4, and 1.1 wt.% since the material becomes more homogeneous with higher thermal input and the iron-based component is predominant. The content of oxide phases in transition from mode 1 to mode 2 decreases insignificantly (by 0.3 wt.%), from 3.2 to 2.9 wt.%.

After examining the structure and properties of the coatings deposited from the wires with 70 B₄C + 30 (Cr, Fe)₇C₃ and 50 B₄C + 50 (Cr, Fe)₇C₃ cores, we established that coatings of higher quality (higher hardness) were produced at a higher thermal input (mode 2). Their microhardness is 6.25 and 8.6 GPa. These coatings are comparable in quality and hardness with previously studied PAS coatings that were sprayed from wires with WC–Co, WC–ZrO₂ (nano), B₄C, and B₄C + ZrO₂ (nano) cores and had a microhardness of 6.59, 5.02, 6.76, and 6.86 GPa [20, 22]. In supersonic electric arc spraying (PLAZER15-SA-EM unit), the coatings sprayed from the Fe–Cr–C-cored wire have a microhardness varying from 3.9 to 6.1 GPa [17].

CONCLUSIONS

New types of wires with a steel sheath and $n\text{B}_4\text{C} + 100-n(\text{Cr, Fe})_7\text{C}_3$ cores have been developed for plasma arc spraying of coatings with increased wear resistance. Optimum modes of high-speed PAS to produce coatings with low porosity (<2.5%), good adhesion to the substrate, and fine lamellar structure and minimize the decarbonization and oxidation processes have been determined.

The DTA method has been used to simulate interaction between wire components, establish the direction of thermodynamic reactions to form new phases, and predict the phase composition of the coatings (provided that the sprayed material is sufficiently protected in the spraying process).

Metallurgical processes that occur in PAS between the steel sheath and carbide cores have been analyzed. The structurization of coatings deposited in optimum PAS modes has been examined. All coatings have been found to show a fine lamellar structure. Both coatings are based on a ferrite matrix doped with Cr, B, and C and hardened with $\text{Fe}_3(\text{B}, \text{C})$, Cr_2B , and FeCr particulate phases and starting boron carbides.

The phase formation processes differ substantially for the wires with $70 \text{ B}_4\text{C} + 30 (\text{Cr}, \text{Fe})_7\text{C}_3$ and $50 \text{ B}_4\text{C} + 50 (\text{Cr}, \text{Fe})_7\text{C}_3$ cores sprayed in the optimum mode (240 A). When the amount of $(\text{Cr}, \text{Fe})_7\text{C}_3$ increases from 30 to 50 wt.% in the core, the following changes occur in the phase composition: the amount of the matrix phase, α -Fe-based solid solution, decreases from 65.8 to 37.6 wt.% and the weight content of the hardening phases, $\text{Fe}_3(\text{B}, \text{C})$, Cr_2B , B_4C , and FeCr , increases from 28.2 to 59.3%.

These processes increase the hardness of the coatings to 6.25 and 8.60 GPa, which is higher than the hardness of the wire steel sheath by 4 and 5.5 times.

These research efforts open prospects of producing high-quality coatings with high hardness by arc plasma spraying of wires with refractory cores. Such coatings can be used as wear-resistant materials for protection of chemical engineering equipment against abrasive wear, in the production of parts for pumps, compressors, and other machines, and for the recovery of worn parts.

REFERENCES

1. B. Wielage, C. Rupprecht, and G.V. Pokhmurska, "Thermal spray deposition of coatings using cored wires (overview)," *Avtomat. Svarka*, No. 10, 26–30 (2011).
2. M.Yu. Kharlamov, I.V. Krivtsun, V.N. Korzhyk, and S.V. Petrov, "Heating and melting of an anode wire in plasma arc spraying," *Avtomat. Svarka*, No. 5, 5–11 (2011).
3. S.V. Petrov and I.N. Karp, *Air Plasma Spraying* [in Russian], Naukova Dumka, Kyiv (1993), p. 499.
4. V.I. Pokhmurski, M.M. Student, V.M. Gvozdetzki, and G.V. Pokhmurska, "Cored wires developed at the Physical Mechanical Institute for electric arc deposition of coatings (overview)," *Avtomat. Svarka*, No. 9, 52–57 (2011).
5. B. Wielage, K. Bobzin, C. Rupprecht, and M. Brahl, "Thermal spraying—potentials, development, markets," in: *Thermal Spray Bulletin*, German Welding Society Verlag (2008), pp. 30–36.
6. M.Yu. Kharlamov, I.V. Krivtsun, V.N. Korzhyk, S.V. Petrov, and A.I. Demianov, "Mathematical model of arc plasma generated by plasmatron with an anode wire," *Avtomat. Svarka*, No. 12, 15–20 (2007).
7. S.V. Petrov and A.G. Saakov, *Combustion Plasma in Surface Engineering* [in Russian], TOPAS, Kyiv (2000), p. 220.
8. M.Yu. Kharlamov, I.V. Krivtsun, V.N. Korzhyk, and S.V. Petrov, "Formation of liquid metal film at the anode wire end in plasma arc spraying," *Avtomat. Svarka*, No. 12, 3–18 (2011).
9. V.I. Pokhmurski, G.V. Pokhmurska, M.M. Student, Yu.V. Dzioba, and Ya.Ya. Sirak, "Cored wire for producing composite thermal spray coatings," *Ukrainian Patent 20013*, IPC (2006) C23C 4/04, C3C 4/12; patent appl. hold. Fiz. Mekh. Inst. NAN Ukrainy, U2006 06217; appl. June 5, 2007; publ. January 15, 2007; Bulletin No. 1.
10. V.I. Pokhmurski, M.M. Student, V.M. Dovgunyk, I.I. Sidorak, Yu.M. Kuskov, and I.M. Riabtsev, "Structure and tribotechnical characteristics of coatings produced by electric arc metal deposition using cored wires," *Avtomat. Svarka*, No. 8, 13–17 (2003).
11. A. Pokhmurska, M. Student, E. Bielanska, and E. Beltowska, "Tribological properties of arc sprayed coatings obtained from FeCrB and FeCr based powder wires," *Surf. Coat. Technol.*, **151–152**, 490–494 (2002).
12. V.I. Pokhmurski, M.M. Student, V.M. Dovgunyk, and I.I. Sidorak, "Cored wires in the $\text{FeCrB} + \text{Al}$ and $\text{FeCr} + \text{Al} + \text{C}$ systems for arc sprayed recovery coatings," *Avtomat. Svarka*, No. 3, 28–31 (2002).
13. V.A. Frolov, V.A. Poklad, B.V. Riabenko, and D.V. Viktorenkov, "Process features of supersonic thermal gas spraying processes (overview)," *Svar. Proizv.*, No. 11, 38–47 (2006).

14. M.M. Student, G.V. Pokhmurska, Ya.Ya. Sirak, and V.M. Gvozdetski, “Cored wire for producing wear-resistant electric arc coatings,” *Ukrainian Patent 40723U*, IPC (2009) C23C 4/00, B22F 7/00, B32B 15/00; patent appl. hold. Fiz. Mekh. Inst. NAN Ukrainy; appl. November 3, 2008; publ. April 27, 2009; Bulletin No. 8.
15. A. Hasui and O. Morigaki, *Cladding and Coating* [Russian translation], Mashinostroenie, Moscow (1981), p. 192.
16. V.N. Korzhyk, I.V. Krivtsun, S.V. Petrov, and M.Yu. Kharlamov, “New Plazer process for renovating railway parts,” *Remont Vosstan. Moderniz.*, No. 1, 20–22 (2009).
17. V.N. Korzhyk, N.P. Lyutik, A.A. Chaika, V.I. Tkachuk, I.D. Gos, and Yu.A. Nikitiuk, “Supersonic electric arc spraying of responsible parts for railway rolling stock,” *Avtomat. Svarka*, No. 9, 20–28 (2016).
18. V.N. Korzhyk and M.F. Korob, “PLAZER 30PL-W mechanized line for plasma arc wire spraying of coatings,” *Svarshchik*, No. 4(86), 13–16 (2012).
19. I.K. Pokhodnya, V.N. Shlepakov, and V.F. Alter, *Production of Cored Wire* [in Russian], Vysshaya Shkola, Kyiv (1980), p. 231.
20. G.M. Grigorenko, L.I. Adeeva, A.Yu. Tunik, V.N. Korzhyk, S.N. Stepaniuk, L.K. Doroshenko, A.A. Chaika, N.P. Lyutik, and L.T. Eremeeva, “Metallurgical processes in plasma arc spraying of coatings using a steel wire with WC and WC–Co powder cores,” *Sovr. Elektrometall.*, No. 4, 14–24 (2015).
21. G.M. Grigorenko, V.N. Korzhyk, A.A. Chaika, L.I. Adeeva, and A.Yu. Tunik, “Structure and properties of supersonic plasma arc coatings hardened with particles from wires with WC and WC + NbC powder cores,” *Tekhnol. Syst.*, No. 2, 26–36 (2016).
22. G.M. Grigorenko, V.N. Korzhyk, L.I. Adeeva, and A.Yu. Tunik, “Metallurgical processes in plasma arc spraying of coatings using a steel wire with B₄C and B₄C+ZrO₂ cores,” *Visn. Priazov. Derzh. Tekh. Univ.*, No. 32, 125–137 (2016).
23. G.M. Grigorenko, L.I. Adeeva, A.Yu. Tunik, V.N. Korzhyk, and L.M. Kapitanchuk, “Structure of plasma arc coatings producing using steel wires with B₄C and nano-ZrO₂ cores,” *Avtomat. Svarka*, No. 9, 23–32 (2017).
24. G.M. Grigorenko, A.L. Borisova, Yu.S. Borisov, L.I. Adeeva, L.K. Doroshenko, and V.L. Rupchev, “Study of phase interaction of ferrotitanium and boron carbide in powder mixtures for thermal spraying of coatings,” *Sovr. Elektrometall.*, No. 1, 28–31 (2003).
25. V.F. Tkachenko and Yu.I. Kogan, “Structural characteristics and mechanical properties of sintered Fe–B₄C materials,” *Powder Metall. Met. Ceram.*, **17**, No. 5, 384–388 (1978).
26. N.F. Nevar, Yu.N. Fasevich, V.M. Senkov, and G.V. Pavlovich, “Structure and commercial application of boron-containing alloy,” *Litie Metall.*, No. 2, Part 2, 174–178 (2005).
27. V.G. Samsonov and I.M. Vinnitski, *Refractory Compounds: Handbook* [in Russian], Metallurgiya, Moscow (1976), p. 560.